Strontium-based metal-organic framework/alendronate-silk fibroin hydrogels promote tendon-bone interface healing

TAO YANG[1*], HANJI ZHANG[1*], MINGJUN LI[2], YIMING REN[1], YUNBO SUN[1], WEIYU HOU[1] and MENGQIANG TIAN[1]

[1]Department of Joint and Sports Medicine, Tianjin Union Medical Center, The First Affiliated Hospital of Nankai University, Tianjin 300121, P.R. China; [2]Hebei Key Laboratory of Biomaterials and Smart Theranostics, Center for Health Science and Engineering, School of Health Sciences and Biomedical Engineering, Hebei University of Technology, Tianjin 300130, P.R. China

Received November 17, 2025; Accepted May 13, 2026

DOI: 10.3892/mmr.2026.13936

Abstract. Rotator cuff tears (RCTs) represent a common orthopedic injury. Poor healing of the tendon-bone interface (TBI) represents a notable challenge for the surgical repair of RCTs. In the present study, silk fibroin (SF)-based hydrogels were prepared for use in RCT repair, which were combined with strontium (Sr)-based metal organic frameworks (Sr/MOFs) that were loaded with or without alendronate sodium (Aln). The efficacy of SF-based hydrogels was evaluated using *in vitro* and *in vivo* experiments. The results of the present study showed that Sr/MOFs exhibited regular rod-like morphology, uniform element distribution and high Aln-loading efficiency. SF + Sr/MOF and SF + Sr/MOF-Aln hydrogels exhibited notable biocompatibility and antioxidant activity, and enhanced the osteogenic differentiation of bone marrow mesenchymal stem cells. *In vivo*, compared with the SF and control groups, the SF + Sr/MOF-Aln group significantly enhanced the maximum load and stiffness of repaired tissues, improved bone microstructure, and promoted the formation of more organized collagen fibers and fibrocartilage at the TBI. Osteogenic stimulation at the TBI using Sr/MOFs and Aln represents a clinically relevant strategy for improving rotator cuff repair outcomes. The findings of the present study provide a novel and clinically promising biomaterial-based therapeutic strategy for enhancing TBI regeneration and improving surgical outcomes following rotator cuff repair.

Correspondence to: Dr Mengqiang Tian, Department of Joint and Sports Medicine, Tianjin Union Medical Center, The First Affiliated Hospital of Nankai University, 190 Jieyuan Road, Tianjin 300121, P.R. China
E-mail: mengqiang_tian@126.com

*Contributed equally

Key words: rotator cuff repair, strontium-based metal-organic frameworks, silk fibroin hydrogel, tendon-bone interface healing, osteogenesis

Introduction

Rotator cuff tears (RCTs) represent a prevalent orthopedic condition that exhibits notable morbidity and affects the quality of life of numerous individuals, particularly the elderly (1). The rotator cuff comprises the tendons of the teres minor, supraspinatus, infraspinatus and subscapularis muscles. It plays an important role in regulating the stability and movement of the shoulder joint, and injury to the rotator cuff may lead to pain, weakness and impaired joint mobility (2). Treatment for RCTs typically involves surgical repair, but the healing process after surgery is complex and may be hindered by various factors, including the age of the patient, fat infiltration, tear size, and the quality of the repaired tendons and bones (3).

One of the predominant challenges in rotator cuff repair is the poor healing ability of the tendon-bone interface (TBI), which is important for restoring the structural and functional integrity of the rotator cuff (4). The TBI has a unique structure that is difficult to replicate and conventional surgery often leads to poor healing and a high risk of re-tear (5). Metal organic frameworks (MOFs) represent a category of porous materials constructed from metal ions or clusters that are connected to each other by organic ligands through coordination bonds (6). Due to their high surface area, adjustable pore size and capacity for modification, MOFs have attracted notable attention in the biomedical field (7). MOFs can be designed to deliver various therapeutic agents to the site of injury in a controlled manner (8), and can also serve as scaffolds to promote cell adhesion, proliferation and differentiation, which are important processes for TBI healing (9). In addition, MOFs have been shown to serve a notable role in alleviating the local accumulation of reactive oxygen species (ROS), which is also considered to be important for promoting TBI repair (10-12). Furthermore, recent studies have highlighted the ability of MOFs to biomineralize biomolecules, offering an additional layer of bioactive protection that further supports cellular functions, and improves the stability and therapeutic efficacy of encapsulated cargo (13,14).

Strontium (Sr) exhibits notable osteogenic properties that enhance TBI healing (15,16). In the present study, a hydrogel was prepared by combining silk fibroin (SF) and Sr-based MOFs (Sr/MOFs) loaded with alendronate sodium (Aln)

(Sr/MOF-Aln). It was hypothesized that this hydrogel would exhibit notable osteogenic activity and promote healing at the TBI in animal models, thus resulting in a structure closer to the natural TBI.

Materials and methods

Preparation of MOFs. Sr/MOFs were synthesized using a previously reported method (17). $SrCl_2 \cdot 6H_2O$ (0.58 g; 2.2 mmol), H_2BDC (0.32 g; 1.93 mmol) and 56 ml dimethylformamide (DMF) were mixed together and stirred. This solution was then stored in a polytetrafluoroethylene-lined stainless-steel container at 100˚C for 2 days. After cooling to room temperature, the synthesized MOFs were filtered, washed with DMF and vacuum-dried at 60˚C.

Preparation of SF hydrogel. An SF hydrogel was prepared as described previously (18). A silkworm cocoon was boiled in 2 l 0.02 M sodium carbonate solution for 1 h, and subsequently boiled in 1 l distilled water for 30 min. The cocoon was then rinsed with fresh distilled water and dried at room temperature in a culture dish for 2 days. Purified SF was dissolved in 9.3 M lithium bromide at 70˚C for 1 h, which was then filtered and dialyzed with distilled water at room temperature for 48 h. After being concentrated with polyethylene glycol (20,000 g/mol), the dialysis tube was cleaned and SF was collected and stored at 4˚C. SF hydrogel was prepared by mixing 1 ml SF solution, 100 μl HRP solution (Beijing Solarbio Science & Technology Co., Ltd.) and 65 μl hydrogen peroxide (H_2O_2) solution (Shanghai Aladdin Biochemical Technology Co., Ltd.).

Sample characteristics. Sr/MOF morphology was characterized via field emission scanning electron microscopy (SEM; Sigma 500; Zeiss GmbH) after being sputter-coated with a thin layer of gold (19). High angle annular dark field scanning transmission electron microscopy combined with energy dispersive spectroscopy was used for elemental mapping (20). The powder samples were dispersed in ethanol via ultrasonication (40 kHz for 5 min at 25˚C) and drop-cast onto a carbon-coated copper grid prior to observation. The X-ray diffraction (XRD) pattern was recorded on an equipped X-ray diffractometer (D8 Discover; Bruker Corporation) (21). To determine the optimal MOF concentration, a series of MOF suspensions with varying concentrations (200, 300, 400, 500, 600, 700 and 800 μg/ml) were prepared. The concentration of Sr from these different groups was evaluated at predetermined time points (days 1, 4, 7, 14 and 21) using inductively coupled plasma mass spectrometry (ICP-MS) (iCAP RQ; Thermo Scientific; Thermo Fisher Scientific, Inc.) (22).

Aln loading. A total of 30.5 mM (8.2 g) Aln was dissolved in 50 ml methanol. Subsequently, 2 ml Aln solution (1.22 mM) was mixed with 100 mg prepared Sr/MOFs and placed on a magnetic stirrer for 48 h (37˚C; 600 rpm) (23). The stirred mixture was then transferred to a centrifuge and centrifuged for 10 min at 12,000 x g at room temperature. This was followed by the removal of the supernatant to obtain the centrifuged product. After repeated washing with deionized water and methanol, the reactants were dried overnight in a vacuum freeze dryer to remove the solvent and subsequently stored at room temperature for further experiments. The success of Aln loading was confirmed via high-performance liquid chromatography (HPLC) (1260 LC system; Agilent Technologies, Inc.). The chromatographic separation was performed at a column temperature of 40˚C using an ACQUITY UPLC HSS T3 column (1.8 μm, 2.1x100 mm; Waters Corporation). The mobile phase consisted of solvent A (10 mM ammonium acetate containing 0.1% formic acid) and solvent B (acetonitrile) at a flow rate of 0.300 ml/min, with a sample injection quantity of 10.0 μl. A total of 400 μg/ml Sr/MOF-Aln was dissolved in distilled water and HPLC analysis was performed at different time points (0, 4, 14, 15 and 18 min) to detect the sustained release of Aln.

Isolation and culture of bone marrow mesenchymal stem cells (BMSCs). Following induction of anesthesia with 4% isoflurane, which was maintained with 2% isoflurane, 6 female Sprague Dawley (SDa) rats (age, 3-4 weeks; weight, 40-60 g; Charles River Laboratories, Inc.) were euthanized by cervical dislocation. The animals were housed in a controlled environment with a temperature of 22±2˚C, relative humidity of 50±10% and under a 12-h light/dark cycle. The rats were provided *ad libitum* access to standard rodent chow and water throughout the duration of the study. Primary rat BMSCs were subsequently isolated from the femoral and tibial bone marrow cavities of euthanized rats (24). BMSCs were cultured in a complete culture medium comprising DMEM (Gibco; Thermo Fisher Scientific, Inc.) supplemented with 1% penicillin-streptomycin (Gibco; Thermo Fisher Scientific, Inc.) and 10% fetal bovine serum (Wisent Biotechnology). BMSCs were cultured in an incubator at 37˚C with 5% CO_2 and the culture medium was changed every 3 days. The BMSCs were obtained for the present study only.

Cell proliferation. Firstly, 96-well plates were pre-coated with 50 μl/well of the respective hydrogels (SF, SF + Sr/MOF and SF + Sr/MOF-Aln) and incubated at 37˚C for 24 h. Subsequently, the wells were washed with a PBS solution. Primary BMSCs (passage 3) were then harvested, and a total of $1x10^3$ BMSCs were added to each well corresponding to the different treatment groups and cultured at 37˚C in a 5% CO_2 incubator. The culture medium was changed on days 1, 3 and 5. Subsequently, the original culture medium was discarded and the cells were incubated with culture medium containing 10% Cell Counting Kit-8 (CCK-8) solution (Abbkine Scientific Co., Ltd.) for 1 h at 1, 4 and 7 days of culture. Following this incubation, 100 μl culture medium was taken from each well and added to a new 96-well plate, after which, optical density values were detected using a microplate reader (Model 680; Bio-Rad Laboratories, Inc.) at 450 nm absorbance (25).

Cytotoxicity assay. BMSCs were seeded into 96-well plates, which were pre-coated with SF hydrogel at 37˚C for 24 h, at a density of $1x10^3$ cells/well. After 48 h of incubation at 37˚C, the cell survival rate was measured using the Calcein AM/PI dual staining kit (cat. no. C2015S; Beyotime Biotechnology) according to the manufacturer's instructions. The culture medium was replaced with a working solution and incubated at 37˚C with 5% CO_2. Subsequently, an inverted fluorescence

microscope (MF53-N; Guangzhou Micro-shot Technology Co., Ltd.) was used to observe the cells and capture images.

Measurement of intracellular ROS. BMSCs were seeded into 96-well plates, which were pre-coated with SF hydrogel at 37˚C for 24 h, at a density of $1x10^3$ cells/well. Subsequently, 100 μM H_2O_2 was added to the culture medium and cells were stimulated at 37˚C for 24 h, whereas cells in the control group were cultured in normal medium without H_2O_2 treatment. Cells were incubated with a 2',7'-dichlorodihydrofluorescein diacetate (DCFH-DA) probe (Beyotime Biotechnology) at 37˚C in 5% CO_2 for 20 min and ROS levels were measured according to the manufacturer's instructions. Fluorescence images were obtained for each group using an inverted fluorescence microscope (MF53-N; Guangzhou Micro-shot Technology Co., Ltd.).

In vitro osteogenic test. To determine whether MOF-based hydrogels promoted osteogenesis, alkaline phosphatase (ALP) activity (at weeks 1 and 2) and extracellular-matrix mineralization (at weeks 2 and 3) were evaluated using ALP (cat. no. P0321S; Beyotime Biotechnology) and Alizarin Red staining kits (cat. no. C0148S; Beyotime Biotechnology), respectively, according to the manufacturer's instructions. For quantification, a total of 100 μl of the respective reaction solution from each sample was transferred to a new 96-well plate. Subsequently, a microplate reader (Model 680; Bio-Rad Laboratories, Inc.) was utilized to measure the absorbance at 410 nm for ALP activity and 560 nm for mineralization.

Reverse transcription-quantitative PCR (RT-qPCR). BMSCs were seeded into 96-well plates pre-coated with SF hydrogel at 37˚C for 7 days. Total RNA was extracted from cells using TRIzol® reagent (Invitrogen; Thermo Fisher Scientific, Inc.) according to the manufacturer's instructions. cDNA was synthesized from 500 ng total RNA using the PrimeScript™ RT Reagent Kit (Takara Bio, Inc.) according to the manufacturer's protocol. Subsequently, qPCR was performed using SYBR Green Master Mix (Takara Bio, Inc.) on a StepOnePlus™ Real-Time PCR System (Applied Biosystems; Thermo Fisher Scientific, Inc.) to detect the expression levels of runt-related transcription factor 2 (Runx2), osteocalcin (OCN), collagen type I α1 chain (COL1A1) and collagen type II α1 chain (COL2A1). The primers used are presented in Table I. The amplification protocol consisted of an initial denaturation step at 95˚C for 30 sec, followed by 50 cycles of denaturation at 95˚C for 5 sec and amplification at 60˚C for 30 sec. GAPDH was used as the internal reference gene. All reactions were conducted in triplicate and relative gene expression levels were calculated using the $2^{-\Delta\Delta Cq}$ method and normalized to the control group (26).

Surgical treatment of the rat RCT model. A rat RCT model was established to evaluate the ability of MOF-based hydrogels to promote RCT repair *in vivo* according to a previously described method (27). In the present study, 48 female SDa rats (age, 4-5 months; weight, 300-350 g; Charles River Laboratories, Inc.) were randomly divided into the following four groups: i) Control group (n=12); ii) SF group (n=12); iii) SF + Sr/MOF group (n=12); and iv) SF + Sr/MOF-Aln group (n=12). This sample size was consistent with previously reported studies on rat models of RCT and TBI healing (28,29). The allocation of rats to each group was concealed using opaque envelopes to ensure that the researchers conducting the experiment were blinded to group assignments, preventing any bias in the outcome assessment.

Table I. Primers used for reverse transcription-quantitative PCR.

Primer	Sequence, 5'-3'
GAPDH	
F	GGAATCCACTGGCGTCTTCA
R	GGTTCACGCCCATCACAAAC
Runx2	
F	CCACAGAGCTATTAAAGTGA
R	AACAAACTAGGTTTAGAGTCATCAAGC
OCN	
F	GGTGCAGACCTAGCAGACACCA
R	AGGTAGCGCCGGAGTCTATTCA
COL1A1	
F	GCATCAGGGTTTCAGAGCA
R	CGTTGGGTCATTTCCACAT
COL2A1	
F	CCCCTGCAGTACATGCGG
R	CTCGACGTCATGCTGTCTCAAG

COL1A1, collagen type I α1 chain; COL2A1, collagen type II α1 chain; F, forward; OCN, osteocalcin; R, reverse; Runx2, runt-related transcription factor 2.

Initially, rats were anesthetized with isoflurane (induction, 4%; maintenance, 2%). Subsequently, the deltoid muscle was exposed under sterile conditions and incised to access the supraspinatus muscle. The supraspinatus tendon was then carefully dissected from its insertion site on the humeral bone using a surgical blade. A tunnel was drilled into the greater tubercle of the humerus and, for experimental groups, the relevant hydrogel was inserted into the tunnel. Finally, the supraspinatus tendon was secured back to the greater tubercle using a non-absorbable suture. Rats in the control group underwent simple suturing of the supraspinatus tendon to the humerus without the addition of any hydrogel. Rats in the SF group were subject to suturing with the incorporation of SF hydrogel at the interface. Similarly, the SF + Sr/MOF group received suturing with the addition of the SF + Sr/MOF hydrogel at the interface, whereas the SF + Sr/MOF-Aln group were sutured with insertion of the SF + Sr/MOF-Aln hydrogel at the interface. Rats were administered aspirin (100 mg/kg; once daily postoperatively for 3 days) via oral gavage to manage pain (30).

The rats were housed in a controlled environment that was maintained at a temperature of 22±2˚C, relative humidity of 50±10% and subject to a 12-h light/dark cycle. All rats were provided *ad libitum* access to standard rodent chow and water throughout the duration of the study. Rats exhibiting signs of notable weight loss (>20% baseline body weight),

an inability to move or infection were humanely euthanized immediately. After 8 weeks, the rats were sacrificed by cervical dislocation under anesthesia, which was induced with 4% isoflurane and maintained with 2% isoflurane. Of these, 6 rats per group were allocated for micro-MRI, micro-CT and biomechanical testing, whereas samples from the remaining 6 rats per group were used exclusively for histological analysis.

Micro-MRI evaluation. Imaging of the supraspinatus tendon-bone complex was performed using a 9.4 T BioSpec 94/30 MRI scanner and positron emission tomography insert (Bruker Corporation). Image acquisition and reconstruction were processed using ParaVision software (version 6.0.1; Bruker Corporation). MRI images of each sample were independently evaluated and graded by two radiologists who were both blinded to the group allocation of the animals. MRI images of the supraspinatus tendon-bone complex were assessed using a semi-quantitative grading system, which included the following three parameters: i) Signal intensity; ii) tendon thickness; and iii) tendon retraction. The detailed grading criteria for sample signal intensity, tendon thickness and tendon retraction are provided in Table SI (31). To ensure the reliability of MRI scoring, inter- and intra-observer consistency were evaluated by calculating the intraclass correlation coefficient based on the assessments of two independent, blinded observers.

Micro-CT evaluation. Imaging of shoulder joint samples was performed using a micro-CT system (Quantum GX2; PerkinElmer, Inc.) with a scanning resolution of 18 μm at a voltage of 50 kV and a current of 100 μA. Image reconstruction and analysis were performed using the Quantum GX2 software (version 2.0; PerkinElmer, Inc.). The parameters analyzed included bone volume/tissue volume (BV/TV) and bone mineral density (BMD), which were quantified according to a previously described method (32).

Biomechanical testing. Samples of the supraspinatus tendon-humerus complex were collected from SDa rats for biomechanical testing using a universal testing machine (UTM6104; Shenzhen SUNS Technology Co. Ltd.) (27). The maximum load (N) and load deformation curve at the time of failure were recorded. The stiffness (N/mm) of each specimen was determined by the slope of the linear region of the load deformation curve until the point of maximum load failure (33). Biomechanical parameters were intentionally reported without normalization to the cross-sectional area of the samples, as successful TBI healing is typically accompanied by an increase in tissue volume; therefore, non-normalized values more accurately reflect the functional repair outcome (33).

Histopathological observation. On the day of sacrifice in week 8, supraspinatus TBI samples from each group were fixed in 4% neutral buffered formalin at room temperature for 48 h. Following dehydration, the samples underwent decalcification for ~60 days. Subsequently, specimens were vertically sectioned and embedded in paraffin wax to obtain tissue blocks with a thickness of ~5 μm using a Leica SP1600 microtome (Leica Microsystems, Inc.). Tissue sections were stained with toluidine blue at room temperature for 5 min to evaluate morphological changes in newly formed fibrocartilage (33). Additional sections were stained with hematoxylin and eosin (H&E) at room temperature for 5 min to assess the maturation of the repaired rotator cuff tissues. Images were captured using a light microscope (Leica TCS SP2; Leica Microsystems, Inc.). Finally, tendon maturation scores were determined using a modified scoring system adapted from a previous study (28). Specifically, this system evaluates five distinct histological parameters: Cellularity, vascularity, continuity, fibrocartilage and tidemark. Each parameter is graded on a scale of 0 to 4, yielding a cumulative total score with a maximum possible value of 20 for each sample.

Statistical analysis. All data in the present study were analyzed using SPSS 17.0 statistical software (SPSS, Inc.). Continuous data are presented as the mean ± standard deviation, and comparisons between groups were conducted via one-way ANOVA followed by Tukey's post hoc test. Categorical data, such as the histological maturation scores and semi-quantitative MRI scores, are presented as the median and interquartile range, and were evaluated using the non-parametric Kruskal-Wallis test followed by Dunn's post hoc test for multiple comparisons. All experiments were independently repeated three times to ensure the reliability of the results. $P<0.05$ was considered to indicate a statistically significant difference.

Results

Characteristics of MOFs. In order to obtain information regarding the microstructure of Sr/MOFs, both Sr/MOF and Sr/MOF-Aln were analyzed by SEM, as shown in Fig. 1A. Sr/MOFs were found to be rod-shaped, indicating that they exhibited notable crystalline morphology. Elemental mapping illustrated the uniform distribution of each element detected within the Sr/MOFs. When loaded with Aln, the phosphorus signal of Sr/MOFs markedly increased, indicating that the loading of Aln onto MOFs was successful (Fig. 1A). The XRD pattern of the synthesized Sr/MOFs also reflected a notable crystal structure, indicating that functional MOFs had been successfully synthesized (Fig. 1B). Upon loading with Aln, no shifts in diffraction peaks were observed. However, observed changes in the Bragg reflectance intensity ratio may have been caused by variations in interatomic distance and bond angle or the preferential orientation of Aln particles. The ICP-MS results demonstrated a general concentration-dependent increase in Sr ion release as the Sr/MOF concentration rose from 200 to 700 μg/ml. For visual conciseness, only the statistical comparisons between the higher concentration groups (600 vs. 700 μg/ml and 700 vs. 800 μg/ml) are explicitly indicated in Fig. 1C. Specifically, significant differences were observed between the 600 and 700 μg/ml groups at days 1, 4,7 and 21. Notably, there was no statistical difference in Sr ion release between the 700 and 800 μg/ml groups at days 1, 4, 7, 14 and 21, indicating that the ion release reached a distinct plateau at concentrations above 700 μg/ml (Fig. 1C). Therefore, a MOF concentration of 700 μg/ml was selected for use in

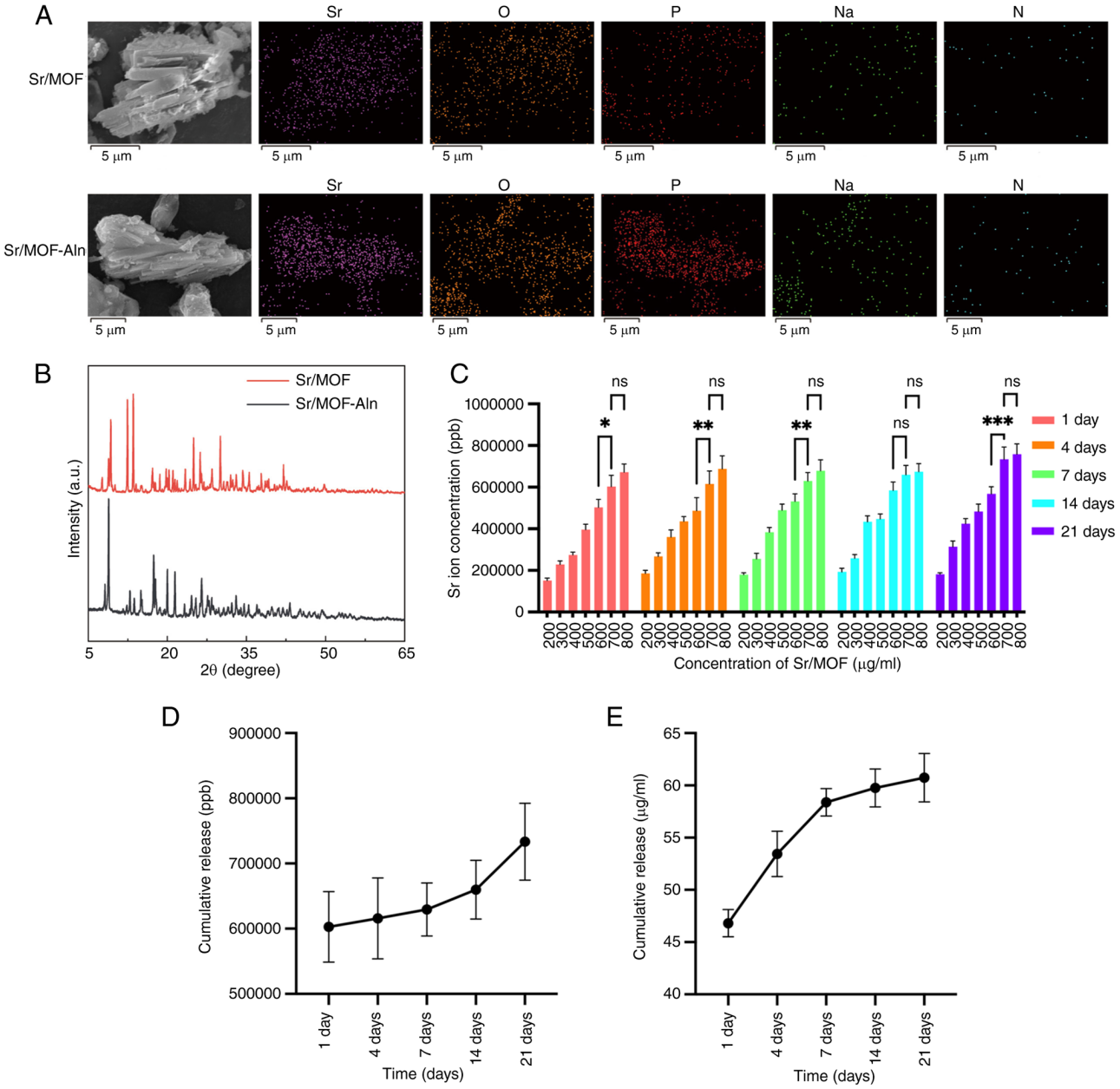

Figure 1. (A) Scanning electron microscopy and corresponding elemental mapping of Sr/MOF and Sr/MOF-Aln. (B) X-ray diffraction patterns of Sr/MOF and Sr/MOF-Aln. (C) Inductively coupled plasma mass spectrometry analysis of Sr ion concentration at different Sr/MOF concentrations. (D) Cumulative release of Sr^{2+} ions from 700 μg/ml Sr/MOF was measured at different time points over a 21-day period. (E) Cumulative release of Aln from Sr/MOF-Aln was measured at different time points over a 21-day period. **P<0.01 and ***P<0.001. Aln, alendronate sodium; a.u., arbitrary units; MOF, metal organic framework; N, nitrogen; Na, sodium; ns, no statistically significant difference; O, oxygen; P, phosphorus; ppb, parts per billion; Sr, strontium.

SF hydrogels in later experiments. HPLC results revealed that MOFs loaded with Aln exhibited the same pattern of peaks as Aln, indicating that the MOFs were successfully loaded with Aln (Fig. S1). Further analysis indicated that the drug loading capacity of Sr/MOFs with Aln reached 39% (data not shown). Subsequently, Sr^{2+} ion release was detected via HPLC. The cumulative release of Sr^{2+} ions increased progressively over the 21-day period, with larger increases in cumulative release observed on days 14 and 21 compared with earlier time points (Fig. 1D). The cumulative release of Aln from Sr/MOF-Aln also increased over the 21-day period; however, this release became more gradual at later time points compared with earlier time points (Fig. 1E).

Hydrogel promotes osteogenic differentiation of BMSCs in vitro. The osteogenic properties of the SF + Sr/MOF group were investigated by measuring the ALP activity of BMSCs. The present study found that ALP staining increased in intensity between 1 and 2 weeks, demonstrating that the degrees of mineralization and osteogenic differentiation increased with time (Fig. 2A). In addition, compared with in the SF group, the ALP activity of BMSCs in the SF + Sr/MOF group significantly increased after 1 and 2 weeks of co-culture, and ALP activity in the SF + Sr/MOF-Aln group was significantly higher than the SF + Sr/MOF group after 2 weeks (Fig. 2B). In addition, the mineralization activity was evaluated to detect osteogenic differentiation status in weeks 2 and 3, with the staining

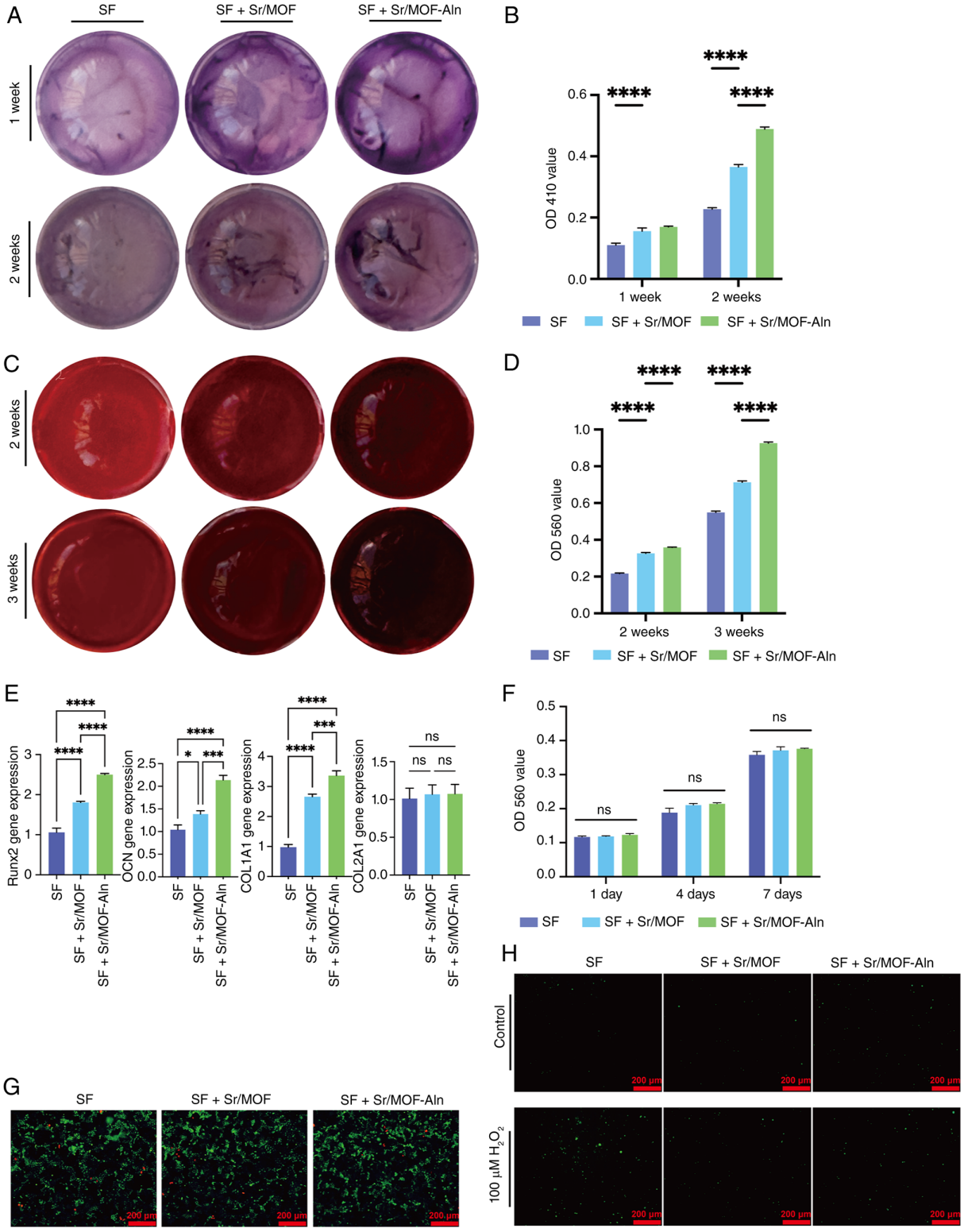

Figure 2. (A) ALP staining of BMSCs after co-culture with hydrogels for 1 and 2 weeks. (B) Quantification of ALP activity at 1 and 2 weeks. (C) Alizarin Red staining of BMSCs to detect extracellular matrix mineralization after co-culture of cells with hydrogels for 2 and 3 weeks. (D) Quantitative mineralization analysis. (E) Relative mRNA expression levels of Runx2, OCN, COL1A1 and COL2A1 in different experimental groups. (F) Analysis of cell proliferation via Cell Counting Kit-8 assay after co-culture of BMSCs with hydrogels for 1, 4 and 7 days. (G) Live/dead staining of BMSCs using Calcein AM/PI following a 48-h incubation with SF hydrogels. (H) Representative images of 2',7'-dichlorodihydrofluorescein diacetate staining for detection of intracellular reactive oxygen species. *P<0.05, ***P<0.001 and ****P<0.0001. Aln, alendronate sodium; ALP, alkaline phosphatase; BMSCs, bone marrow mesenchymal stem cells; COL1A1, collagen type I α1 chain; COL2A1, collagen type II α1 chain; H_2O_2, hydrogen peroxide; MOF, metal organic framework; ns, no statistically significant difference; OCN, osteocalcin; Runx2, runt-related transcription factor 2; SF, silk fibroin; Sr, strontium.

intensity of cells gradually increasing over time (Fig. 2C). Furthermore, quantitative analysis confirmed a significantly higher mineralization degree in the SF + Sr/MOF group at both time points, as evidenced by the increased OD values

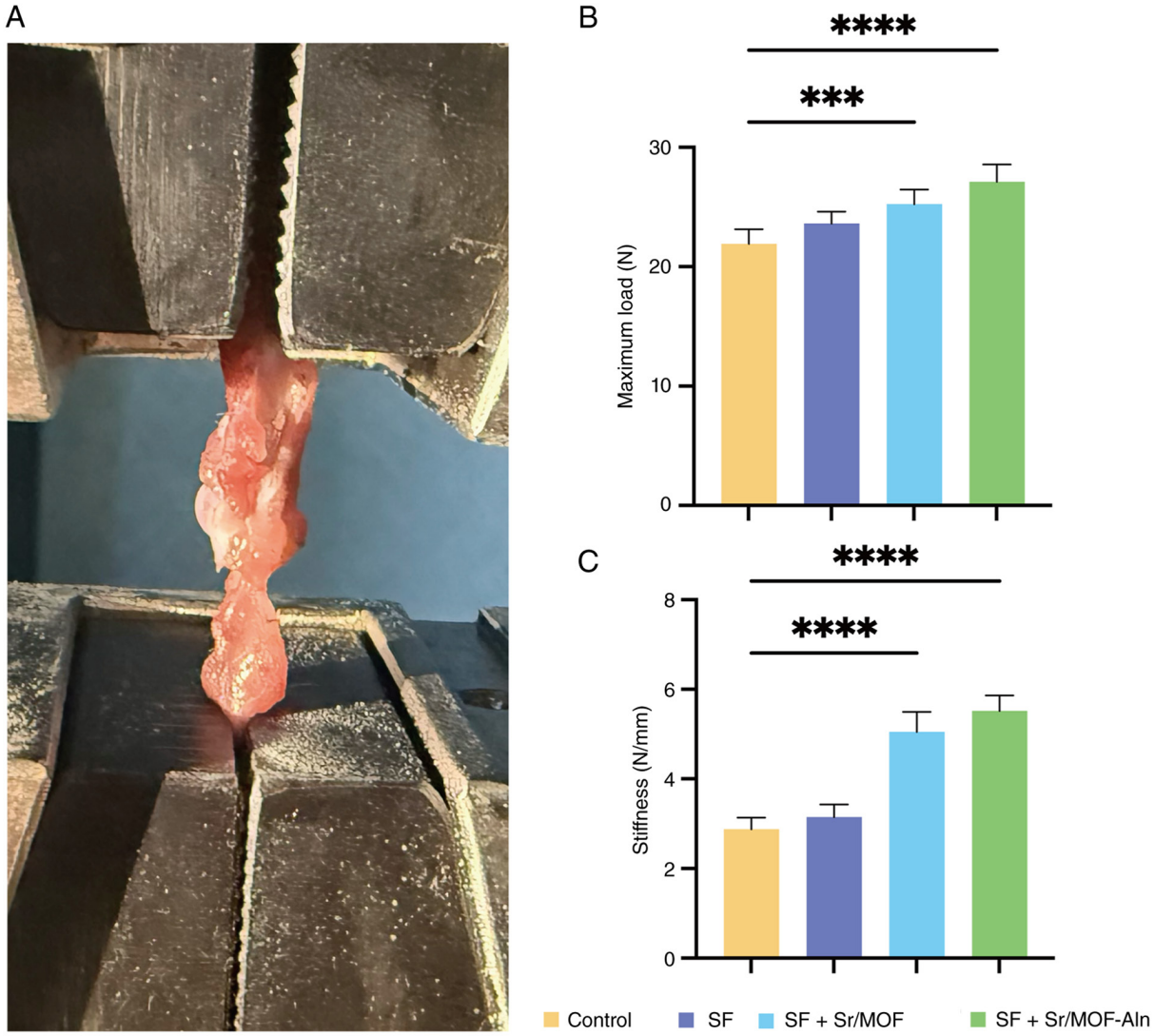

Figure 3. (A) Representative image of the experimental setup for biomechanical testing of the supraspinatus tendon-humerus complex. (B) Maximum load and (C) stiffness values of the control, SF, SF + Sr/MOF and SF + Sr/MOF-Aln groups. ***P<0.001 and ****P<0.0001. Aln, alendronate sodium; MOF, metal organic framework; SF, silk fibroin; Sr, strontium.

(Fig. 2D). Additionally, the SF + Sr/MOF-Aln group exhibited denser mineral nodules and significantly higher mineralization levels compared with in the SF + Sr/MOF group at both time points. Furthermore, the expression levels of Runx2, OCN and COL1A1 gradually increased across the three experimental groups (Fig. 2E). Specifically, the SF + Sr/MOF group exhibited significantly increased gene expression levels compared with the SF group, whereas the SF + Sr/MOF-Aln group demonstrated the highest expression levels. By contrast, COL2A1 expression remained consistent across all treatment groups, demonstrating no statistically significant differences.

Biocompatibility of hydrogel. According to CCK-8 assay results, compared with in the SF group, the SF + Sr/MOF and SF + Sr/MOF-Aln groups demonstrated no significant differences in proliferation rate after incubation for 1, 4 and 7 days (Fig. 2F). Additionally, according to the results of calcein AM/PI staining, no notable differences in cell survival rate were observed between groups after 48 h of treatment (Fig. 2G).

Antioxidant properties of hydrogels. The present study subsequently investigated whether SF + Sr/MOF or SF + Sr/MOF-Aln could reduce the increase in ROS caused by H_2O_2. Analysis of DCFH-DA staining revealed that the proportion of cells that stained positive for ROS following H_2O_2 treatment were increased compared with in the untreated control group. In addition, compared with the H_2O_2 + SF group, the relative number of BMSCs that stained positively for ROS was markedly reduced in the H_2O_2 + SF + Sr/MOF and SF + Sr/MOF-Aln groups (Fig. 2H).

Biomechanical testing. Biomechanical testing of the collected SDa rat supraspinatus tendon-humerus complexes was performed via a universal testing machine (Fig. 3A). After 8 weeks of rotator cuff tendon repair, the maximum load values in the SF + Sr/MOF and SF + Sr/MOF-Aln groups were significantly increased compared with in the control group (Fig. 3B). The stiffness of rotator cuffs across the four groups also showed similar results; the stiffness values gradually increased from the control group to the SF + Sr/MOF-Aln

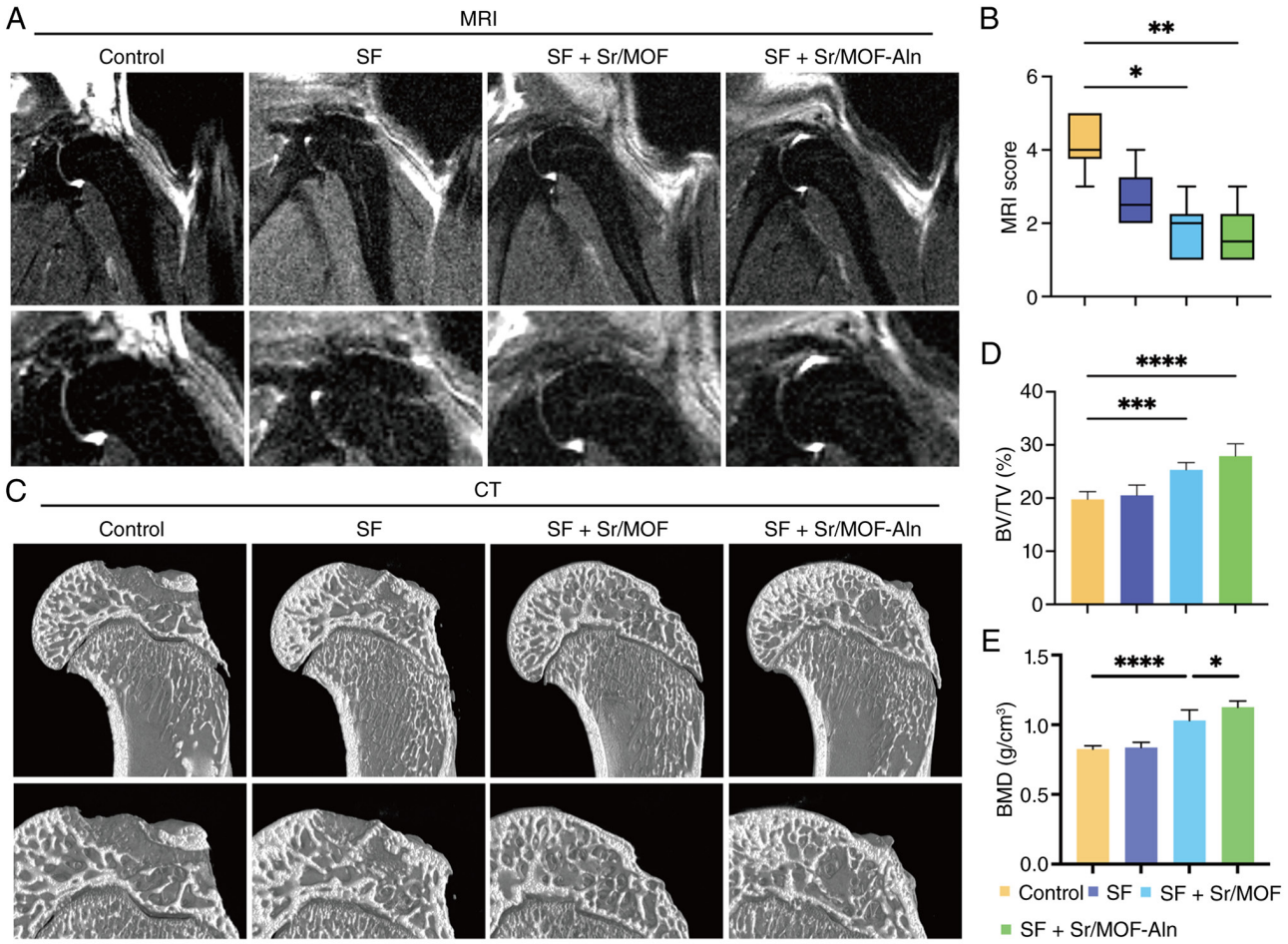

Figure 4. (A) Representative micro-MRI images of the supraspinatus tendon-bone complex and (B) MRI scores in the control, SF, SF + Sr/MOF and SF + Sr/MOF-Aln groups, with higher scores indicating poorer healing. (C) Representative micro-CT images of new bone formation close to the hydrogel implantation site. Quantitative analysis of (D) BV/TV and (E) BMD. *P<0.05, **P<0.01, ***P<0.001 and ****P<0.0001. Aln, alendronate sodium; BMD, bone mineral density; BV/TV, bone volume/tissue volume; MOF, metal organic framework; SF, silk fibroin; Sr, strontium.

group, and a significant difference was observed between the control group and the SF + Sr/MOF group (Fig. 3C). In addition, a significant increase in rotator cuff stiffness was observed between the control group and the SF + Sr/MOF-Aln group.

Imaging evaluation. A total of 8 weeks after rotator cuff surgery, rats were examined using a micro-MRI system to observe the healing of the TBI (Fig. 4A). Subsequently, CT imaging of rat shoulder joints was used to examine bone repair at the TBI (Fig. 4C). Analysis of the regeneration status of tendons was evaluated using an MRI scoring system, in which higher MRI scores corresponded with poorer TBI healing. The control group scored the highest, followed by the SF and SF + Sr/MOF groups, whereas the SF + Sr/MOF-Aln group had the lowest MRI score (Fig. 4B). Notably, compared with in the control group, the MRI scores of the SF + Sr/MOF and SF + Sr/MOF-Aln groups were significantly decreased. However, the difference between the SF group and the control group was not statistically significant, and no significant differences were observed among the three treatment groups (SF, SF + Sr/MOF and SF + Sr/MOF-Aln) (Fig. 4B). Micro-CT images were used to generate 3D reconstructions of the humerus bones of rats in order to evaluate the growth of new bone tissue in each treatment group. There was no statistically significant difference in BV/TV and BMD between the control group and the SF group (Fig. 4D and E). However, the BV/TV and BMD values of the SF + Sr/MOF group were significantly increased compared with in the control group and the BMD of the SF + Sr/MOF-Aln group was significantly increased compared with the SF + Sr/MOF group, which indicated that the loading of Sr/MOFs with Aln was therapeutically effective.

Histological analysis. In order to observe the microstructure after surgery, the local tissues were stained and analyzed. H&E staining indicated that collagen fibers in the SF + Sr/MOF-Aln group appeared to be more organized compared with the other treatment groups (Fig. 5A). According to tendon maturation score, the SF + Sr/MOF group showed a significant increase in tendon maturity 8 weeks after RCT surgery compared with in the control group (Fig. 5B). Toluidine blue staining was used to evaluate newly formed fibrocartilage, as shown in Fig. 5C. While cartilage matrix deposition was limited in the control group, the SF + Sr/MOF and SF + Sr/MOF-Aln groups exhibited a robust and continuous fibrocartilage layer. After 8 weeks, the fibrocartilage area of the SF + Sr/MOF and SF + Sr/MOF-Aln groups was significantly increased compared with the control group (Fig. 5D). These results indicated

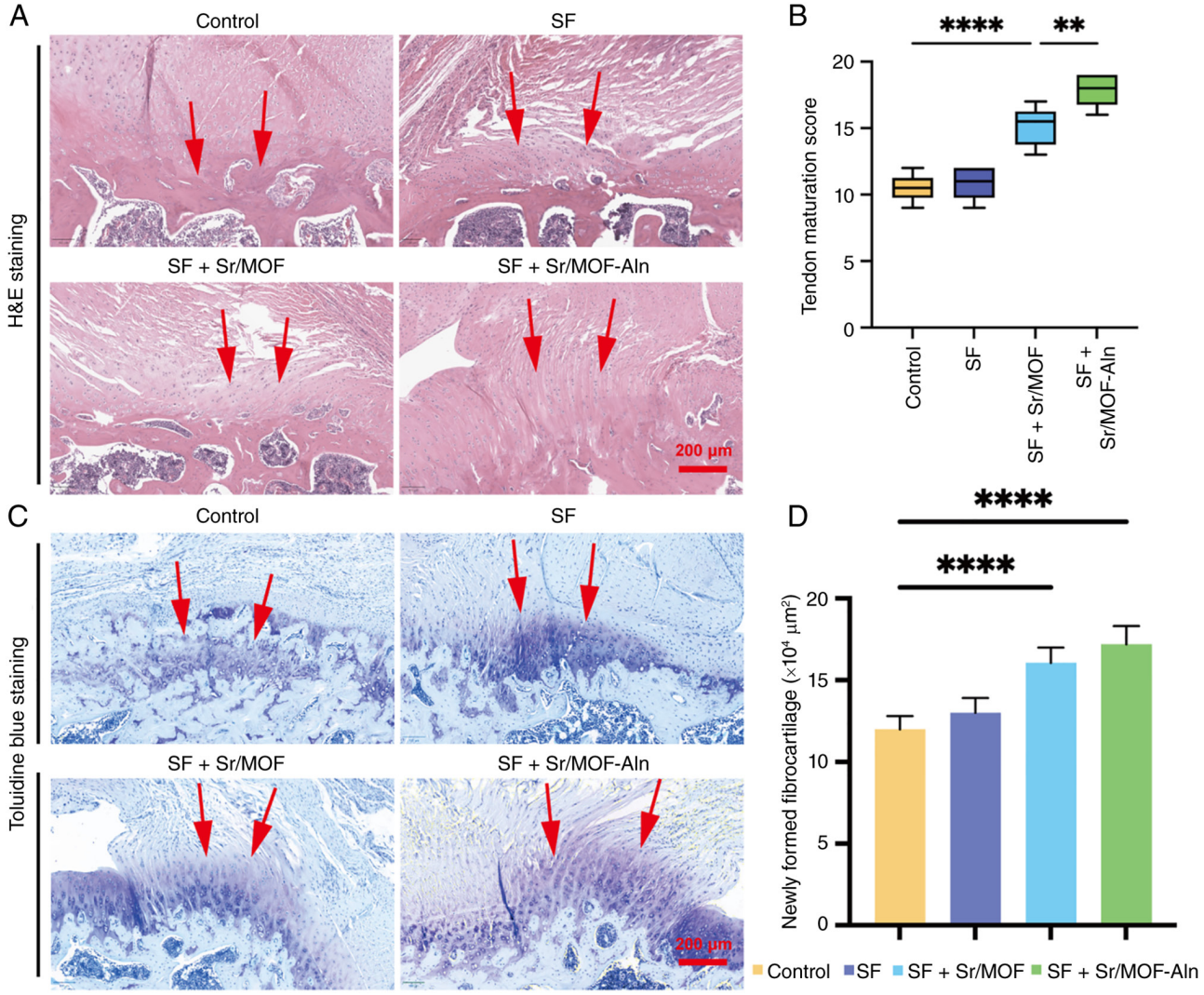

Figure 5. (A) H&E staining of supraspinatus tendon-humerus complex sections (arrows indicate the arrangement of collagen fibers). (B) Tendon maturation scores. (C) Toluidine blue staining of tissue sections for fibrocartilage detection (arrows indicate the newly formed fibrocartilage). (D) Quantitative analysis of fibrocartilage area in supraspinatus tendon-humerus complex samples. **P<0.01 and ****P<0.0001. Aln, alendronate sodium; H&E, hematoxylin and eosin; MOF, metal organic framework; SF, silk fibroin; Sr, strontium.

that, compared with in the other treatment groups, the SF + Sr/MOF-Aln group may have demonstrated an improved ability to repair RCTs.

Discussion

In the present study, an SF-based hydrogel was prepared and combined with Sr/MOFs loaded with or without Aln for use in RCT repair. The therapeutic efficacy of different hydrogel treatments was validated through comprehensive *in vitro* and *in vivo* evaluations.

Sr/MOFs exhibited a clear rod-shaped morphology, uniform element distribution and stable crystal structure, as well as high Aln-loading efficiency and controlled Sr^{2+} ion release. *In vitro* experiments revealed that SF + Sr/MOF and SF + Sr/MOF-Aln hydrogels exhibited notable biocompatibility, enhanced osteogenic differentiation and demonstrated marked antioxidant activity. The results of the present study suggested that SF + Sr/MOF hydrogels may have primarily mediated RCT repair by influencing osteogenesis and fibrocartilage formation rather than chondrogenesis. Therefore, these results highlighted the functional impact of Sr/MOF-Aln in enhancing bone regeneration at the TBI.

In vivo, compared with in the SF and control groups, the SF + Sr/MOF-Aln group achieved higher maximum load and stiffness, improved bone microstructure, and enhanced organization of collagen fibers and fibrocartilage at the TBI. Several studies have investigated the use of Sr-based biomaterials and drug-loaded systems for promoting TBI healing (29,34,35). The present study offers unique insights by integrating Sr/MOFs with a SF hydrogel. The present study was, to the best of our knowledge, the first study to apply Sr/MOFs for RCT repair and the results supported the efficacy of Sr/MOFs in promoting TBI healing by utilizing the notable osteogenic properties of MOFs and Sr^{2+} ions. *In vitro*, Sr^{2+} ions were continuously released from Sr/MOF for 21 days, preventing sudden ion release and ensuring sustained osteogenic stimulation. *In vivo*, this sustained release is transformed into enhanced growth of new bone and formation of fibrocartilage at the TBI (36). The osteogenic effect of Sr has been fully supported by previous

studies (15,16). Sr^{2+} ions can activate the Smad/Runx2 signaling pathway and upregulate osteogenic gene expression. Other studies (37,38) have confirmed the ability of Sr to balance the activity of osteoblasts and osteoclasts, which is necessary for preventing bone resorption at the repair site. Additionally, Sr exerts notable antioxidant effects by mitigating ROS-related damage, particularly in contexts relevant to musculoskeletal tissue repair (10,12), which is important for TBI healing (11).

MOFs have demonstrated considerable therapeutic advantages when compared with traditional drug carriers in RCT repair. The high porosity and notable specific surface area of MOFs have been shown to facilitate their high drug-loading capacity and adjustable release kinetics (39), and MOFs have been reported to maintain their crystal structure under physiological conditions (39). In addition, MOFs have been shown to lack cytotoxicity towards mammalian cells, which is consistent with the *in vitro* biocompatibility results observed in the present study (40).

Gao *et al* (29) explored the ability of Sr-doped mesoporous bioglass nanoparticles (Sr-MBG) in electrospun fiber scaffolds to promote healing at the TBI. The approach adopted in the aforementioned study highlighted the immune-modulatory effects of Sr-MBG, which promoted macrophage polarization towards the M2 phenotype, and increased the osteogenic and chondrogenic differentiation of mesenchymal stem cells, improving biomechanical strength at the TBI. By contrast, the present study demonstrated that Sr/MOFs integrated with SF hydrogel offer an alternative approach to TBI healing by providing sustained Sr^{2+} ion release and bioactive protection, similarly enhancing regeneration and improving mechanical properties at the TBI. Additionally, Sun *et al* (34) used dissolvable microneedle patches loaded with diacerein nanoparticles to mitigate oxidative stress and promote macrophage polarization towards the M2 phenotype. The results of the aforementioned study aligned with the findings of the present study, demonstrating Sr^{2+} ion-mediated mitigation of ROS-induced damage, enhancing tendon-bone healing. Furthermore, Baker *et al* (35) explored the pharmacological mobilization of endogenous mesenchymal stem cells for rotator cuff repair. The findings of the aforementioned study aligned with the findings of the present study, which showed that Sr/MOF-based hydrogels could enhance cell differentiation and tissue regeneration without the need for exogenous cells, suggesting the therapeutic potential of integrating these hydrogels with mesenchymal stem cell mobilization strategies for synergistic effects in tendon-bone healing.

The combination of Aln and Sr/MOFs further enhanced the efficacy of RCT repair. This was related to the function of MOFs as drug carriers (39,41), which may enable localized, sustained delivery of therapeutic agents directly to the TBI, thereby maintaining a high local drug concentration while minimizing dissemination to non-target tissues. In the present study, the synergistic effect of Aln and Sr^{2+} ions facilitated bone remodeling and improved the biomechanical strength of regenerated bone, which was measured *in vivo* using micro-CT and biomechanical tests. Yin *et al* (42) provided evidence that Aln treatment in a rat RCT model of osteoporosis improved bone microstructure and reduced the receptor activator of NF-κB ligand/osteoprotegerin ratio, thereby inhibiting excessive osteoclast activity and stabilizing the TBI. This was consistent with the *in vivo* results of the present study, which demonstrated that the SF + Sr/MOF-Aln hydrogel increased bone growth compared with the SF + Sr/MOF group. Abdalla and Pendegrass (43) demonstrated that bisphosphonates can promote TBI healing by reducing bone loss at tendon attachment points, which is important for preventing suture anchor dislodgement. In addition, another study emphasized that when released through local carriers, Aln can regulate local bone metabolism without producing systemic side effects, thereby addressing the limitations of systemic Aln administration (44). In general, the aforementioned studies provided notable evidence supporting the role of Aln in enhancing RCT healing. The findings of the present study supported this role by revealing the synergistic effects of Aln and Sr/MOFs in the hydrogel system.

Although the results of the present study are encouraging, there are several limitations that need to be addressed in future research. Notably, the present study focused primarily on the osteogenic potential of the Sr/MOF-Aln hydrogel and did not assess tenogenic markers, such as scleraxis and tenomodulin, which are important for evaluating tendon regeneration (45). The absence of these markers from the analyses of the present study therefore limited the elucidation of cellular events involved in TBI healing. Although the present study generated quantitative release profiles for both Sr^{2+} ions and Aln over a 21-day period, a correlation analysis between ion or drug release and biological outcomes was not performed. Future studies should incorporate correlation analyses to further elucidate how the release kinetics of Sr^{2+} ions and Aln influence biological responses and to establish a clearer material-function relationship. These analyses would provide valuable insights into the sustained osteogenic stimulation and therapeutic efficacy of the hydrogel system used in the present study. Notably, the *in vivo* experiments of the present study were only established over 8 weeks. However, other studies have evaluated the effectiveness of RCT repair at 12 weeks postoperatively to assess long-term mechanical durability and tissue remodeling at the TBI (29,43). Furthermore, the present study used a healthy rat model of RCTs, but patients with RCT often exhibit osteoporosis, which is a key risk factor for poor TBI healing (42). Testing hydrogels in an RCT model of osteoporosis is necessary to support their applicability in high-risk groups. The present study provided new insights into RCT repair, demonstrating that Sr/MOFs may not only promote bone formation but also may load drugs to further enhance TBI regeneration, establishing avenues for the development of Sr/MOFs that promote TBI healing.

The present study successfully developed multifunctional composite hydrogels by integrating Sr/MOFs, Aln and SF, and systematically verified the efficacy of these hydrogels in RCT repair at the TBI. Both *in vitro* and *in vivo* evaluations systematically confirmed their enhanced efficacy compared with the control and SF-only groups in cytocompatibility, osteogenesis, ROS scavenging and subsequent TBI regeneration. To the best of our knowledge, the present study represented the first application of Sr/MOFs in RCT repair, leveraging the synergistic effects of Sr ions, Aln and the drug-delivery capability of MOFs on TBI healing to address the notable challenge of RCT treatment. The composite SF + Sr/MOF-Aln hydrogel provided a novel, efficient and biocompatible strategy for promoting

rotator cuff repair, laying a foundation for the development of advanced biomaterials for promoting TBI regeneration and demonstrating the promising translational potential of Sr/MOF hydrogels for use in clinical orthopedic practice.

Acknowledgements

The authors would like to thank Dr Jiahao Luo (Hebei University of Technology) for his assistance in the experiments.

Funding

The present study was supported by the Foundation of Tianjin Union Medical Center (grant no. 2020YJ009) and the Tianjin Science and Technology Major Special Projects (grant nos. 21 ZXJBSY00080 and 25ZXSWSY00370).

Availability of data and materials

The raw ICP-MS data generated in the present study have been deposited in the iProX repository under accession number PXD077411 or at the following URL: https://www.iprox.cn/page/project.html?id=IPX0016720000. The other data generated in the present study may be requested from the corresponding author.

Authors' contributions

MT and TY designed the study. TY and HZ performed the experiments. ML, YR, YS, WH and MT analyzed data. MT and TY confirm the authenticity of all the raw data. All authors contributed to the writing of the manuscript. MT and TY revised the manuscript. All authors read and approved the final manuscript.

Ethics approval and consent to participate

All animal procedures were examined and approved by The Animal Ethics Committee of Nankai University (approval no. 2025-SYDWLL-000288).

Patient consent for publication

Not applicable.

Competing interests

The authors declare that they have no competing interests.

References

1. Yamamoto A, Takagishi K, Osawa T, Yanagawa T, Nakajima D, Shitara H and Kobayashi T: Prevalence and risk factors of a rotator cuff tear in the general population. J Shoulder Elbow Surg 19: 116-120, 2010.
2. Neviaser A, Andarawis-Puri N and Flatow E: Basic mechanisms of tendon fatigue damage. J Shoulder Elbow Surg 21: 158-163, 2012.
3. Quinlan NJ, Hillyard B, Wheelwright JC, Miller M, Kawakami J, Tashjian RZ and Chalmers PN: Footprint size matters: Wider coronal greater tuberosity width is associated with increased rates of healing after rotator cuff repair. JSES Int 5: 486-492, 2021.
4. Zhao S, Su W, Shah V, Hobson D, Yildirimer L, Yeung KWK, Zhao J, Cui W and Zhao X: Biomaterials based strategies for rotator cuff repair. Colloids Surf B Biointerfaces 157: 407-416, 2017.
5. Turcotte JJ, Kelly M, West M, Lashgari C, Petre BM and Redziniak DE: Rates of medial and lateral row failure and risk factors for Re-tear in arthroscopic double row rotator cuff repair. J Clin Orthop Trauma 36: 102083, 2022.
6. Nguyen LM, Wang Y, Quynh Vu GT, Hoai Ta QT, Tran DL, Nguyen NH, Van Tran T, Zhang C and Nguyen DH: The synergy of metal-organic frameworks and biomaterials for bone tissue engineering: Recent advances, challenges, and future recommendations. Nanoscale Adv 7: 5479-5500, 2025.
7. Yang R, Zheng Y, Zhang Y, Li G, Xu Y, Zhang Y, Xu Y, Zhuang C, Yu P, Deng L, *et al*: Bipolar metal flexible electrospun fibrous membrane based on metal-organic framework for gradient healing of tendon-to-bone interface regeneration. Adv Healthc Mater 11: e2200072, 2022.
8. Khafaga DSR, El-Morsy MT, Faried H, Diab AH, Shehab S, Saleh AM and Ali GAM: Metal-organic frameworks in drug delivery: Engineering versatile platforms for therapeutic applications. RSC Adv 14: 30201-30229, 2024.
9. Li X, Shu X, Shi Y, Li H and Pei X: MOFs and bone: Application of MOFs in bone tissue engineering and bone diseases. Chinese Chemical Letters 34: 107986, 2023.
10. Han C, Zhang M, Xu S, Wang C, Li B and Zhao W: Strontium ranelate-loaded human hair keratin-hyaluronic acid hydrogel accelerates wound repair with anti-inflammatory and antioxidant properties. Int J Biol Macromol 281 (Pt 4): 136536, 2024.
11. Kim RJ, An SH, Gwark JY and Park HB: Antioxidant effects on hypoxia-induced oxidative stress and apoptosis in rat rotator cuff fibroblasts. Eur Cell Mater 41: 680-693, 2021.
12. Shen X, Fang K, Ru Yie KH, Zhou Z, Shen Y, Wu S, Zhu Y, Deng Z, Ma P, Ma J and Liu J: High proportion strontium-doped micro-arc oxidation coatings enhance early osseointegration of titanium in osteoporosis by anti-oxidative stress pathway. Bioact Mater 10: 405-419, 2021.
13. Zhou JN, Liu C, Wang Y, Guo Y, Xu XY, Vuorimaa-Laukkanen E, Koivisto O, Filppula AM, Ye J and Zhang H: Biomineralize mitochondria in metal-organic frameworks to promote mitochondria transplantation from non-tumorigenic cells into cancer cells. Smart Med 4: e134, 2025.
14. Faheem A, Lawrence MC, Bushra GA, Meli MV and Blight BA: Metal-organic frameworks as anchors for giant unilamellar vesicle immobilization. J Mater Chem B 13: 2317-2326, 2025.
15. Kuang GM, Yau WP, Lu WW and Chiu KY: Local application of strontium in a calcium phosphate cement system accelerates healing of soft tissue tendon grafts in anterior cruciate ligament reconstruction: Experiment using a rabbit model. Am J Sports Med 42: 2996-3002, 2014.
16. Kuang GM, Yau WP, Lu WW and Chiu KY: Use of a strontium-enriched calcium phosphate cement in accelerating the healing of soft-tissue tendon graft within the bone tunnel in a rabbit model of anterior cruciate ligament reconstruction. Bone Joint J 95-B: 923-928, 2013.
17. Li Z, Peng Y, Xia X, Cao Z, Deng Y and Tang B: Sr/PTA metal organic framework as a drug delivery system for osteoarthritis treatment. Sci Rep 9: 17570, 2019.
18. Pierantoni L, Ribeiro VP, Costa L, Pina S, da Silva Morais A, Silva-Correia J, Kundu SC, Motta A, Reis RL and Oliveira JM: Horseradish peroxidase-crosslinked calcium-containing silk fibroin hydrogels as artificial matrices for bone cancer research. Macromol Biosci 21: e2000425, 2021.
19. Wei X, Wang M, Dong X, He Y, Nan W, Ji S, Zhao M, Chang H, Wei H, Ding D and Chen H: Internal-External homologous drug-loaded exosome-like nanovesicles released from Semi-IPN hydrogel enhancing wound healing of chemoradiotherapy-induced oral mucositis. Int J Nanomedicine 20: 4105-4121, 2025.
20. Liu S, Dun C, Yang F, Tung KL, Wierzbicki D, Ghose S, Chen K, Chen L, Ciora R, Khan MA, *et al*: A general flame aerosol route to kinetically stabilized metal-organic frameworks. Nat Commun 15: 9365, 2024.
21. Donnadio A, Paul G, Barbalinardo M, Ambrogi V, Pettinacci G, Posati T, Bisio C, Vivani R and Nocchetti M: Immobilization of alendronate on zirconium phosphate nanoplatelets. Nanomaterials (Basel) 13: 742, 2023.
22. Reiner T, Sorbi R, Müller M, Nees T, Kretzer JP, Rickert M and Moradi B: Blood metal ion release after primary total knee arthroplasty: A prospective study. Orthop Surg 12: 396-403, 2020.

23. Xue X, Yu J, Lu F, Jiang H and Wang X: Enhancement of cancer chemotherapeutic efficacy via bone-targeted drug delivery carrier in bone metastases. Drug Des Devel Ther 15: 4455-4468, 2021.
24. Zhang W, Zheng L, Yan Y and Shi W: Facile preparation of multifunctional hydrogels with sustained resveratrol release ability for bone tissue regeneration. Gels 10: 429, 2024.
25. Ren J, Duan H, Dong H, Wu S, Du Y, Zhang G and Zhang A: TAT nanobody exerts antiviral effect against PRRSV in vitro by targeting viral nucleocapsid protein. Int J Mol Sci 24: 1905, 2023.
26. Livak KJ and Schmittgen TD: Analysis of relative gene expression data using real-time quantitative PCR and the 2(-Delta Delta C(T)) method. Methods 25: 402-408, 2001.
27. Ren Y, Zhang S, Wang Y, Jacobson DS, Reisdorf RL, Kuroiwa T, Behfar A, Moran SL, Steinmann SP and Zhao C: Effects of purified exosome product on rotator cuff tendon-bone healing in vitro and in vivo. Biomaterials 276: 121019, 2021.
28. Wu B, Zhang T, Chen H, Shi X, Guan C, Hu J and Lu H: Exosomes derived from bone marrow mesenchymal stem cell preconditioned by low-intensity pulsed ultrasound stimulation promote bone-tendon interface fibrocartilage regeneration and ameliorate rotator cuff fatty infiltration. J Orthop Translat 48: 89-106, 2024.
29. Gao H, Wang L, Lin Z, Jin H, Lyu Y, Kang Y, Zhu T, Zhao J and Jiang J: Bi-lineage inducible and immunoregulatory electrospun fibers scaffolds for synchronous regeneration of tendon-to-bone interface. Mater Today Bio 22: 100749, 2023.
30. The Forsyth Institute: Administration of Analgesia in Rats and Mice. The Forsyth Institute, Somerville, MA, 2021. https://www.google.com/url?sa=t&source=web&rct=j&opi=89978449&url=https://forsyth.org/wp-content/uploads/2025/05/Analgesia.pdf&ved=2ahUKEwiso9zGpfeUAxX6hf0HHaJYLz8QFnoECBoQAQ&usg=AOvVaw0XXKs-mz3aP7JdLpbt8-qI
31. Ross D, Maerz T, Kurdziel M, Hein J, Doshi S, Bedi A, Anderson K and Baker K: The effect of granulocyte-colony stimulating factor on rotator cuff healing after injury and repair. Clin Orthop Relat Res 473: 1655-1664, 2015.
32. Wang HT, Li J, Ma ST, Feng WY, Wang Q, Zhou HY, Zhao JM and Yao J: A study on the prevention and treatment of murine calvarial inflammatory osteolysis induced by ultra-high-molecular-weight polyethylene particles with neomangiferin. Exp Ther Med 16: 3889-3896, 2018.
33. Renhao Y, Gen L, Chengyu Z, Yang R, Li G, Zhuang C, Yu P, Ye T, Zhang Y, Shang P, *et al*: Gradient bimetallic ion-based hydrogels for tissue microstructure reconstruction of tendon-to-bone insertion. Sci Adv 7: eabg3816, 2021.
34. Sun J, Chen QZ, Hong AZ, Ju F, Wang HL, Zhang B, Liu W, Sun YC, Tan J, Yang QQ and Zhou YL: Dissolvable microneedle-assisted transdermal administration of diacerein nanoparticles achieved satisfactory therapeutic effects in tendon-bone insertion repair by reducing oxidative stress and inflammation. Mater Today Bio 33: 101999, 2025.
35. Baker KC, Fleischer M, Newton MD, Galasso L, Cavinatto L, Weisz KM, Hartner S, Maerz T, Lammlin L, Baker EA, *et al*: Pharmacologic mobilization and chemokine-directed recruitment of mesenchymal stromal cells to the surgically repaired rotator cuff. Am J Sports Med 53: 1806-1816, 2025.
36. Thomopoulos S, Matsuzaki H, Zaegel M, Gelberman RH and Silva MJ: Alendronate prevents bone loss and improves tendon-to-bone repair strength in a canine model. J Orthop Res 25: 473-479, 2007.
37. Ma P, Chen T, Wu X, Hu Y, Huang K, Wang Y and Dai H: Effects of bioactive strontium-substituted hydroxyapatite on osseointegration of polyethylene terephthalate artificial ligaments. J Mater Chem B 9: 6600-6613, 2021.
38. Chen T, Wu X, Zhang P, Wu W, Dai H and Chen S: Strontium-doped hydroxyapatite coating improves osteo/angiogenesis for ameliorative graft-bone integration via the macrophage-derived cytokines-mediated integrin signal pathway. ACS Appl Mater Interfaces 16: 15687-15700, 2024.
39. Xie X, Wang Y, Li Z, Yang G, Cheng G, Qin S, Wang H and Zhu L: Recent advances in gradient biomimetic scaffolds for tendon-bone interface regeneration. Front Bioeng Biotechnol 13: 1629816, 2025.
40. Zhu C, Lv Y, Qian C, Qian H, Jiao T, Wang L and Zhang F: Proliferation and osteogenic differentiation of rat BMSCs on a novel Ti/SiC metal matrix nanocomposite modified by friction stir processing. Sci Rep 6: 38875, 2016.
41. Guan H, Ding F, Xue Y and Zhao J: Engineering the mechanical characteristics of regenerated silk fibroin materials: the impact of chemical and physical modification strategies. Front Chem 13: 1606995, 2025.
42. Yin H, Ding Y, Feng Z, Yan Z and Guo A: Quantitative computed tomography analysis of bone microarchitecture is associated with rotator cuff healing. J Orthop Surg Res 20: 670, 2025.
43. Abdalla AA and Pendegrass CJ: Biological approaches to the repair and regeneration of the rotator cuff tendon-bone enthesis: A literature review. Biomater Transl 4: 85-103, 2023.
44. Song L, Li N and Chen J: Research advances in mesenchymal stem cells and related therapies for rotator cuff tendon-to-bone healing. Front Bioeng Biotechnol 13: 1647909, 2025.
45. Kubo Y, Hoffmann B, Goltz K, Schnakenberg U, Jahr H, Merkel R, Schulze-Tanzil G, Pufe T and Tohidnezhad M: Different frequency of cyclic tensile strain relates to anabolic/catabolic conditions consistent with immunohistochemical staining intensity in tenocytes. Int J Mol Sci 21: 1082, 2020.